New experiments and theory on ferrofluid cylinder in an azimuthal magnetic field

R. Canu, A. Bouchet, M.-C. Renoult

Accepted to Phys. Fluids 10.1063/5.0169793

New experiments and theory on ferrofluid cylinder in an azimuthal magnetic field

R. Canu,[1] A. Bouchet,[1] and M.-C. Renoult*[1]
Normandie Univ, UNIROUEN, INSA Rouen, CNRS, CORIA, 76000 Rouen, France

(*Corresponding author's email: renoultm@coria.fr)

(Dated: 6 October 2023)

We conducted experiments to study the stability of a ferrofluid cylinder in an azimuthal magnetic field. The ferrofluid cylinder is formed on a current-carrying wire for creating the azimuthal magnetic field and is surrounded by a non-magnetic fluid of the same density to neglect the gravitational effect. Experiments were performed for different wire and cylinder radii. Data were analysed to extract the growth rate and the wavelength of the perturbation characterising the ferrofluid cylinder. The influence of the wire radius on the cylinder stability is used to respond to an issue, recently raised, in relation to the growth rate data obtained by the first experimental work. The results of the experiments confirm the theoretical predictions, namely a decrease in the growth rate when the ratio between the wire radius and the ferrofluid cylinder radius increases. However, the isothermal theory overpredicts the growth rate observed in this experiment and sources of this discrepancy are explored. In particular, a theoretical model considering a thermocapillary effect is developed and it is shown that this non-isothermal theory can explain the observed discrepancy.

I. INTRODUCTION

Ferrofluids are electrically non-conducting magnetic liquids composed of solid magnetic nanoparticles dispersed in a carrier liquid phase. They are encountered in various applications in printing, medicine, computer science, robotics, aeronautics and electrical engineering. Due to their magnetic properties, they are influenced by magnetic fields. Depending on the shape of the magnetic field, a perturbation of the ferrofluid may or may not be stabilised.

In this paper, we focus on the stability of a ferrofluid cylinder subjected to a magnetic field and surrounded by a non-magnetic fluid. The azimuthal magnetic field shape, which is stabilising[1], is explored here because it is simple to generate experimentally. A rectilinear wire, with an electrical current passing through it, is placed in the centre of the ferrofluid cylinder. In this way, an azimuthal magnetic field can be created. The presence of the wire influences the cylinder stability. It is therefore important to look at the effect of the wire radius on this stability.

Arkhipenko *et al.*[2] conducted experiments on this case by decreasing the current traversing the wire from a stabilising to a destabilising value. The experimental data reported in their study indicate an increase in the growth rate of the most unstable perturbation when the ratio between the wire radius and the cylinder radius increases. However, the opposite behaviour was predicted by the theory based on linear stability analysis under isothermal conditions (figure 1) of: Arkhipenko *et al.*[2] who took into account the density of the surrounding fluid, Canu and Renoult[3] who considered the viscosity of the ferrofluid, Canu and Renoult[4] who took into account the viscosity of the surrounding fluid; and Ferguson Briggs and Mestel[5] who considered an inhomogeneous magnetic permeability. Bourdin, Bacri, and Falcon[6] also conducted experiments on a ferrofluid cylinder coating a wire but with forced perturbations and at high currents so as to be in a stabilising situation (see Canu and Renoult[3] for more details of the wire effects on stable modes). Nevertheless, these experiments did not solve the issue. New experiments are therefore necessary to conclude on the effect of modifying the wire radius on the cylinder stability.

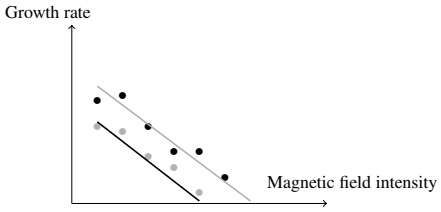

FIG. 1: Schematic representation of the issue regarding the effect of the wire radius. Discs correspond to the experimental data taken from Arkhipenko *et al.*[2] and solid lines correspond to the theoretical predictions of Canu and Renoult[4]. The two colours represent the two different ratios between the wire radius and ferrofluid cylinder radius (0.357 in grey and 0.476 in black).

It has to be noted that the experiments on ferrofluid cylinders are assumed to be conducted under isothermal conditions. But some thermal effects have been reported in the literature, in particular by Arkhipenko *et al.*[7] who noticed the influence of the thermocapillary effect on heated ferrofluid cylinders. The thermocapillary effect has been studied for many configurations such as annular pools[8–11], liquid bridges[12], liquid layers[13–16] and liquid films on inclined planes[17,18]. Regarding liquid columns, which are the configuration of interest of this paper, Xu and Davis[19] showed that the capillary breakup of a liquid jet with an axial temperature gradient is retarded for small Prandtl numbers and large Biot numbers. Hu and Imaishi[20] studied an annular liquid column around a solid fiber and noticed an influence of the thermocapillary mechanism on the liquid radius. Finally, Ryzhkov and Shevtsova[21] observed that a liquid column with an axial temperature gradi-

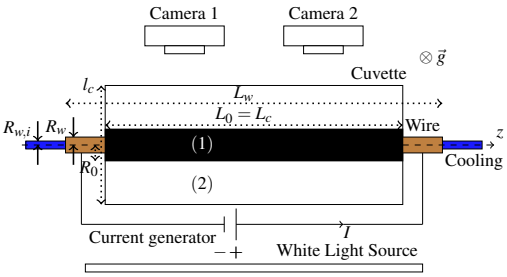

FIG. 2: Top view of the experimental setup. Liquid (1) corresponds to the ferrofluid and liquid (2) corresponds to the surrounding glycerol solution.

ent can be stabilised if the liquid is surrounded by a gas flowing in the opposite direction than the thermocapillary flow. Except for the study of Arkhipenko *et al.*[7], the thermocapillary effect has not been regarded for the case of a ferrofluid cylinder under a magnetic field. Furthermore, Arkhipenko *et al.*[7] have only investigated this case in the limit of a thin layer of ferrofluid and without taking into account the wire cooling and the Joule effect.

In this paper, experiments are performed to investigate the effect of modifying wire radius on the stability of a ferrofluid cylinder subjected to an azimuthal magnetic field. Firstly, the methodology is described: experimental set-up, data acquisition and image analysis. Then, the results are shown with regard to the wavelength and growth rate. The experimental values are compared to the theoretical predictions from the isothermal model that considers the viscosity of the fluids[4] and to a new model developed here that considers a thermocapillary effect. The results allow us to conclude about the issue raised in a previous work and the necessity of better controlling the wire cooling.

II. EXPERIMENTS AND METHOD

The experimental set-up, schematised in figure 2, is composed of a hydromagnetic part and a separate optical part.

A rectangular cuvette of length $L_c = 30\ cm$, width $l_c = 4\ cm$ and height $h_c = 4\ cm$ is used to contain the liquids. The upper face is open to allow the insertion of liquids. The smaller lateral faces are drilled in their centre to allow for the passage of a hollow cylindrical copper wire of inner radius $R_{w,i}$, outer radius R_w and length $L_w = 50\ cm$. Two pairs of values $(R_{w,i}, R_w)$ are used for the radii: $(0.8, 1.0)\ mm$ and $(1.0, 1.5)\ mm$. The wire is connected to two parallel generators delivering a variable current I to create an azimuthal magnetic field. The hollow cylinder can cool the wire by passing cold water through it using a tap in order to dissipate the heat created by the Joule effect.

The ferrofluid used in this experiment is the EMG 905 ferrofluid from the Ferrotec company. The density $\rho_1 = 1170\ kg \cdot m^{-3}$ and the viscosity $\eta_1 = 7.5 \times 10^{-3}\ Pa \cdot s$ are respectively measured by weighing a given volume and using a rotational rheometer (Anton Paar MCR 302e). The relative magnetic permeability $\mu_r = 4.52$ is given by Ferrotec. The surrounding fluid is an aqueous solution with a 77% glycerol concentration. The density $\rho_2 = 1199\ kg \cdot m^{-3}$ is measured with a densimeter (Anton Paar DMA 35) and the viscosity $\eta_2 = 40 \times 10^{-3}\ Pa \cdot s$ is given by tables. The interfacial tension between the ferrofluid and the glycerol solution can only be measured using our tensiometer (Lauda TVT 2) up to a glycerol concentration of 20%. Indeed, for higher glycerol concentrations, the density difference between both liquids was too small for the drop volume method used by the tensiometer. To obtain the value for a concentration of 77%, the data were extrapolated using a logarithmic evolution. This logarithmic law was found using five data points with a mean error of 1%. For the interfacial tension, $\sigma = 0.026\ N \cdot m^{-1}$ is retained. The ferrofluid and the glycerol solution have approximately the same density, like in the Plateau tank technique, to neglect the gravity effect.

Regarding the optical part of the experimental set-up, a light source and diffusion screen are placed behind the cuvette to illuminate it. Two cameras (LaVision Imager Pro X 4M) are used to film the experiment with a frequency $f_t = 13.4666\ Hz$ and a spatial resolution $f_x = 13.44\ px \cdot mm^{-1}$. They are linked to a programmable timing unit to synchronise them. The data are acquired using the DaVis software.

To perform the experiment, the cuvette is filled with the glycerol solution. The hollow wire is linked to the tap to allow cold water to flow inside. Then, the generators are switched on with a high current ($I = 40\ A$) to reproduce the conditions of cylinder stability. The ferrofluid is deposited on the wire with a pipette. The length of the ferrofluid column is therefore equal to the cuvette length $L_c = 30\ cm$ (60% of the wire length). This percentage along with the small aspect ratio of the wire $\Lambda_w = R_w/L_w$ $(0.002 < \Lambda_w < 0.003)$ allows us to determine the azimuthal magnetic field intensity assuming an infinite wire length (see Canu and Renoult[3] for more details). A picture of the ferrofluid column is taken using the DaVis software when it is stable to measure the column radius R_0 using image analysis. The current delivered by the generators is then rapidly decreased manually until the desired value is reached. The ferrofluid column is destabilised and the destabilisation process, which leads to the formation of a drop-on-wire structure, is captured using the DaVis software until the system reaches a state of equilibrium. The current is then increased to $I = 40\ A$ to stabilise the column once again. The experiment, performed at room temperature ($T = 22\ ^\circ C$), is repeated for different current values ($I = \{0; 3; 5; 8; 10; 13; 15; 17\}\ A$), two wire radii ($R_w = \{1; 1.5\}\ mm$) as well as different ferrofluid column radii R_0.

After performing the experiments, the data are analysed. To do this, the images obtained from the DaVis software have to be processed with filters in order to be exploitable. The different steps of the image processing are as follows. The spectrum of the image is first stretched to obtain a better contrast (see figure 3 (top)). An image of the cuvette without the ferrofluid

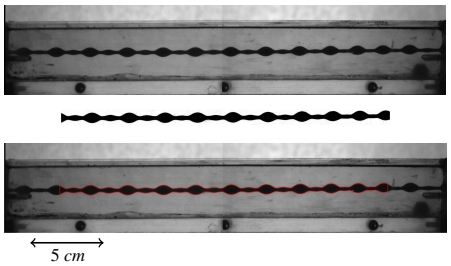

FIG. 3: Case $R_w = 1\ mm$ and $I = 3.1\ A$. (Top) Image of the drop-on-wire structure with a stretched spectrum before processing. (Middle) Image after processing in the region of interest. (Bottom) Image before processing with edge detection.

and wire is taken to remove the background of the processed image. Then, the image is cropped in the region of interest to remove the part of the column close to the cuvette wall which is attracted by capillarity and to remove the elements of the experimental setup. A smoothing filter is used to decrease the noise and a Sobel filter is employed to detect the edge of the ferrofluid column. The image is binarised and the column is filled to obtain an image with the ferrofluid in black and the surrounding fluid in white. Finally, the image is added to that obtained after using the Sobel filter to obtain a grey-level gradient at the edge of the column. The final image after processing is shown in figure 3 (middle). Another python script is used to extract the coordinates of all the points of the ferrofluid column edge (see figure 3 (bottom)). In the first image of each experiment, when the column is still stable, the column radius R_0 is determined by dividing the number of pixels in the radius by the spatial resolution f_x.

To obtain the growth rate of the perturbed surface, two methods are used. The first is based on the temporal evolution of the maximum of each peak of the perturbation. The amplitude a of the perturbation is proportional to $e^{\alpha t}$ in which α is the growth rate and t is the time. Therefore, tracing the logarithm of the amplitude as a function of time, a linear regime is observed whose slope represents the growth rate. The retained value is the average of the growth rates of all the peaks along the ferrofluid column.

The second method involves the temporal evolution of the interface length. In the linear regime of the perturbation, namely for short times, the relation $ln(\Delta L) = 2\alpha t + C$ is observed with ΔL being the difference between the interface length L at time t and the interface length L_0 at the initial time when the column is not deformed, and C being a constant (for more details on the methodology, see Renoult *et al.* [22]).

A typical example for the two methods is shown in figure 4 where the linear regime is well observed. In this figure, the limits are also plotted. The lower limit of 2 pixels shows that the spatial resolution of the camera is sufficient to well capture the linear regime. The upper limits show that the values of the amplitude and the interface length difference are weak enough for using a linear stability analysis. These limits are chosen in order to have a small amplitude compared to the wavelength λ of the perturbation and a small interface length difference compared to $L_0/4$. This second limit can be found using the methodology of Renoult *et al.* [22]. The length of a curve $y(x)$ (here, the interface) in a plane xOy is

$$L = \int_0^{\frac{2\pi n}{k}} \sqrt{1 + \left(\frac{\partial y}{\partial x}\right)^2}\, dx \tag{1}$$

with k the wavenumber and n an integer number. Here y corresponds to the amplitude of the perturbation $a = a_0 cos(kx) e^{\alpha t}$ with a_0 the initial amplitude. Initially, the length is $L_0 = 2\pi n/k$. Considering small t and a_0 (linear analysis), the interface length difference can be approximated by

$$\Delta L \simeq \frac{n\pi k a_0^2}{2} e^{2\alpha t} \tag{2}$$

To obtain this expression, $k^2 a_0^2 e^{2\alpha t} << 1$ has been assumed. Making appear this inequality in the ΔL expression, it follows that $2k\Delta L/(n\pi) << 1$. Recognizing the expression of L_0, the condition $\Delta L << L_0/4$ is obtained.

For the two methods, the first time taken into account for the growth rate calculation is chosen so that all the peaks observed when the perturbation is fully developed are detected by the script at this time for the first time.

Finally, the wavelength of the perturbation is deduced from the position of the maxima of each peak. The retained value is the spatial average when the ferrofluid column seems to be at an equilibrium state.

In the next section, the experimental measurements of the wavelength and the growth rate are compared with the theoretical predictions obtained by Canu and Renoult [4] under isothermal conditions. The equations of the problem were made dimensionless by using the Rayleigh time $\sqrt{\rho_1 R_0^3/\sigma}$, R_0, σ/R_0, the magnetic field intensity $H_0 = I/2\pi R_0$ and the permeability of free space μ_0 as characteristic time, length, pressure, magnetic field and magnetic permeability, respectively. The growth rate values depend on six dimensionless numbers: density ratio $\rho_r = \rho_2/\rho_1$, viscosity ratio $\eta_r = \eta_2/\eta_1$, relative magnetic permeability μ_r, dimensionless wire radius $\delta_w = R_w/R_0$, Ohnesorge number $Oh_1 = \eta_1/\sqrt{\rho_1 \sigma R_0}$, and magnetic Bond number $N_{Bo,m} = \left(\mu_0 (\mu_r - 1) I^2\right) / \left(4\pi^2 \sigma R_0\right)$.

In the experiments presented here, three of these numbers are set as follows: $\rho_r = 1.025$, $\eta_r = 5.33$ and $\mu_r = 4.52$. The three other numbers (δ_w, Oh_1 and $N_{Bo,m}$) vary. Because the aim of this study is to investigate the influence of the dimensionless wire radius on the stability of a ferrofluid cylinder under an azimuthal magnetic field, several series of experiments are performed where R_w and R_0 vary, which thus modify the δ_w value. For each configuration of radii, the current I is varied, thus modifying $N_{Bo,m}$. Three runs are performed for each I. In the experiments, it is preferable to change δ_w by modifying R_w because R_0 also appears in Oh_1 whose modification is not desired in this study. However, R_0 is not accurately controllable in the experiment and its value changes in the different series of measurements. Nevertheless, the Oh_1

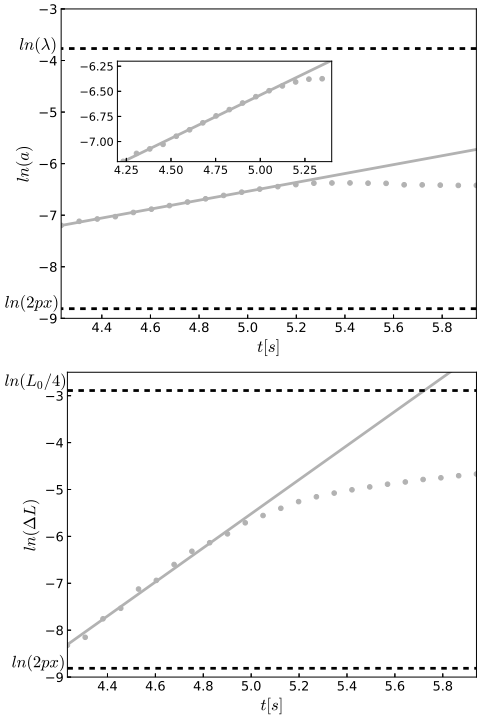

FIG. 4: Calculation of the growth rate with the two methods for the configuration $R_w = 1\ mm$, $R_0 = 2.12\ mm$ and $I = 0\ A$. Top: natural logarithm of the amplitude a of the perturbation for one peak as a function of time with a blow-up of the linear regime. Bottom: natural logarithm of the interface length difference ΔL as a function of time. Circles correspond to the calculated a (top) and ΔL (bottom). Grey straight lines correspond to the linear regression of the linear regime of the curve whose slope is respectively the growth rate $\alpha_1 = 0.863\ s^{-1}$ (top) and twice the growth rate $\alpha_2 = 1.818\ s^{-1}$ (bottom). Black dashed lines correspond to the limits.

variation is very slight and does not avoid the comparison between the different experimental series. It should be noted that the ferrofluid cylinder is stable for all perturbation wavelengths if $N_{Bo,m} \geq 1$. The experiments are conducted in the unstable case, thus for $N_{Bo,m} < 1$. Some of the acquired data were not exploitable either because the initial moments were not always captured on camera or because some peaks merged with others. Furthermore, some data were not provided when the growth rates obtained with the two methods deviated by more than 40%. It was the case for the configuration shown in figure 4 even if it illustrates well the methodology used for growth rates calculation.

TABLE I: Dimensional values for the current I, the theoretical growth rate α_{th} (isothermal model of Canu and Renoult [4]), the experimental growth rate obtained with the first method (peak maximum) α_1, the experimental growth rate obtained with the second method (interface length) α_2, the theoretical wavelength λ_{th} and the experimental wavelength λ. The first, second and third series of measurements are in the first, second and third data block respectively.

$I\ (A)$	$\alpha_{th}\ (s^{-1})$	$\alpha_1\ (s^{-1})$	$\alpha_2\ (s^{-1})$	$\lambda_{th}\ (cm)$	$\lambda\ (cm)$
2.9	4.424	1.627	1.774	2.10	2.32
3.0	4.429	1.449	1.656	2.07	2.07
7.9	3.722	1.047	1.367	2.25	2.44
8.1	3.689	1.073	1.500	2.28	2.68
8.2	3.657	1.157	1.203	2.22	2.42
13.1	2.519	0.769	0.548	2.68	2.58
13.1	2.492	0.780	0.595	2.64	2.68
13.2	2.449	0.779	0.757	2.63	2.64
3.1	4.419	2.422	1.808	1.99	2.28
3.2	4.407	1.576	1.566	2.00	2.28
3.2	4.407	1.430	1.570	2.00	2.28
5.2	4.170	2.148	1.779	2.04	2.26
8.0	3.661	1.067	1.205	2.12	2.23
8.2	3.617	1.643	1.645	2.13	2.24
10.0	3.205	0.520	0.612	2.23	2.50
10.0	3.181	0.889	0.837	2.21	2.52
10.1	3.156	0.995	1.079	2.21	2.89
12.9	2.405	0.750	0.632	2.45	2.61
13.1	2.328	0.275	0.350	2.46	2.78
13.1	2.318	0.646	0.447	2.45	2.79
15.0	1.737	0.222	0.176	2.69	3.28
15.1	1.723	0.208	0.197	2.71	3.27
0.0	2.706	0.443	0.279	2.69	2.58
7.8	2.312	0.457	0.550	2.78	2.64
8.2	2.277	0.424	0.424	2.80	2.92
8.4	2.260	0.361	0.318	2.82	2.83
8.5	2.231	0.377	0.307	2.80	2.68
9.9	2.075	0.461	0.400	2.86	3.10
10.0	2.073	0.512	0.445	2.87	3.15
10.4	2.018	0.501	0.450	2.89	3.15
13.0	1.671	0.412	0.308	3.05	3.16
13.1	1.648	0.360	0.266	3.05	3.19
17.0	1.068	0.217	0.162	3.52	3.50

III. RESULTS: COMPARISON WITH ISOTHERMAL THEORY

In figures 5 and 6, the dimensionless wavelength and the growth rate of the perturbation are shown as a function of the magnetic Bond number for three series of data. The corresponding dimensional values are reported in table I. For the first series (light grey), $R_w = 1\ mm$ and $R_0 = 2.254\ mm$ on average, leading to $\delta_w = 0.444$ and $Oh_1 = 0.029$. For the second series (intermediate grey), $R_w = 1\ mm$ and $R_0 = 2.126\ mm$ on average, leading to $\delta_w = 0.470$ and $Oh_1 = 0.029$. For the third series (black), $R_w = 1.5\ mm$ and $R_0 = 2.861\ mm$ on average,

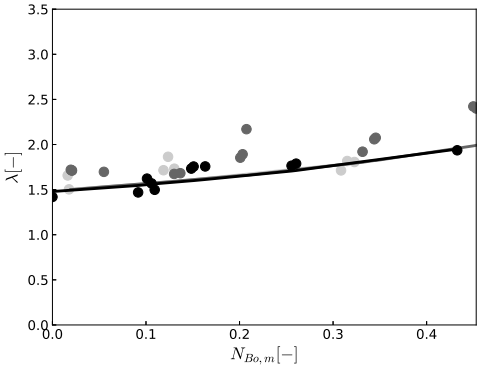

FIG. 5: Value of λ as a function of $N_{Bo,m}$. The viscous theory of Canu and Renoult [4] is represented by solid lines. Circles correspond to the experimental data. Light grey corresponds to the first series of measurements ($\delta_w = 0.444$ on average), intermediate grey to the second series ($\delta_w = 0.470$ on average) and black to the third series ($\delta_w = 0.524$ on average).

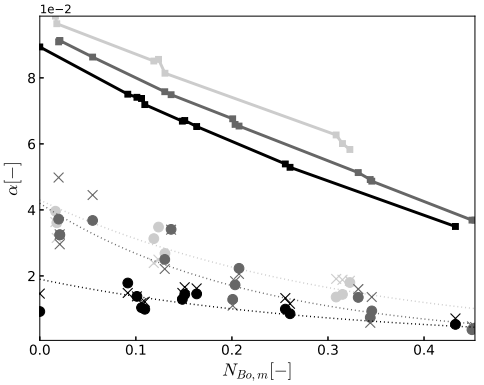

FIG. 6: Value of α as a function of $N_{Bo,m}$. The viscous theory of Canu and Renoult [4] is represented by solid lines with symbols. Crosses correspond to the experimental data obtained using the first method (peak maximum). Circles correspond to the experimental data obtained using the second method (interface length). Dotted lines correspond to the trend curves of the experimental data. Light grey corresponds to the first series of measurements ($\delta_w = 0.444$ on average), intermediate grey to the second series ($\delta_w = 0.470$ on average) and black to the third series ($\delta_w = 0.524$ on average).

leading to $\delta_w = 0.524$ and $Oh_1 = 0.025$. The theoretical predictions shown on the figures and calculated with the isothermal theory of Canu and Renoult [4], are not smooth because the R_0 value varies slightly during the experiments and thus so does δ_w.

Firstly, the wavelength of the perturbation is examined to see if the experimentally observed perturbation corresponds to the theoretically most unstable one. In figure 5, the wavelength of the perturbation (divided by 2π, $\lambda = 1/k$ with k as the dimensionless wavenumber) measured experimentally is compared with the theoretically most unstable one. For the first, second and third series of measurements, the discrepancies between theory and experiment are 6.4%, 14.6% and 4.9% on average respectively. The experimentally observed perturbations are quite similar to the most unstable mode that is weakly dependent on δ_w, showing that the experiments are in the free cylinder configuration as in Arkhipenko *et al.* [2]. In the following, the experimental growth rate measurements will thus be compared to the theoretical growth rate of the most unstable mode.

In figure 6, the tendency of the experimental data confirms the theoretical predictions: for the same $N_{Bo,m}$ value, the dimensionless growth rate of the most unstable mode decreases when δ_w increases. This is more visible when comparing the first and third series because the difference between their δ_w value is more significant.

In a previous work[4], the comparison between theory and the experimental data of Arkhipenko *et al.* [2] revealed an inversion in the influence of the wire radius on the growth rate. This could be due to a typo in the legend of the figure illustrating these results. Thus, these new experiments allow us to resolve an issue raised in the literature about the effect of modifying the wire radius on the cylinder growth rate measurements.

However, in these experiments, a discrepancy is observed between the growth rate predictions and the associated measurements. The predicted growth rate is about 3-4 times higher than the measured growth rate, thus indicating dissipation in our system. In previous experiments, the difference between our predictions and the measurements of Arkhipenko *et al.* [2] was between 10% and 20% on average. The sources for this discrepancy are examined in the following.

Firstly, the cooling of the wire was performed with a constant flow rate of water for all experiments for which the Joule effect may be of different intensity. A temperature gradient, which is not taken into account in the theory, may be present in the ferrofluid and the surrounding fluid, leading to inhomogeneous values of densities, viscosities, interfacial tension and magnetic permeability, or homogeneous values at a different temperature than the room temperature. However, the temperature-related uncertainties on the values of densities, viscosities, interfacial tension and magnetic permeability were shown, thanks to a sensitive analysis of the isothermal theory, not to entirely explain the discrepancy observed in the prediction of the growth rate. Nevertheless, heat transfers could be a source because of the possible temperature gradient in the fluids, as already mentioned above, and the possible unsteady temperature due to the current variations during the passage from stable to unstable configuration. Therefore, a theory that considers these heat transfers should be used.

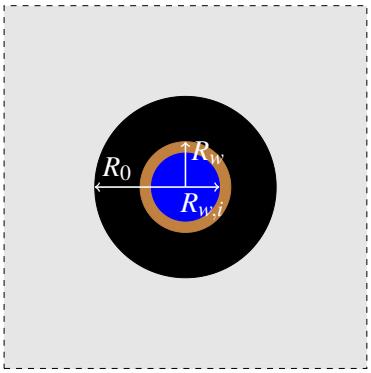

FIG. 7: Cross section of the studied system with water in blue, wire in brown, ferrofluid in black and surrounding fluid in grey.

For the case of a thin layer of ferrofluid, Arkhipenko *et al.* [7] have developed a theory that includes a thermocapillary effect. They showed an influence of this mechanism on the growth rate when the cylinder is heated. They also showed a modification of the stability condition $N_{Bo,m} > 1$, as observed in the present experiments.

To verify if this mechanism could be the source of the discrepancy, a thermal balance is performed in the next section to complete the description of the experiment and a dispersion relation taking into account the thermocapillary effect is derived.

IV. RESULTS: NON-ISOTHERMAL MODEL

As in the work of Canu and Renoult [4], an incompressible Newtonian ferrofluid cylinder of infinite length surrounded by an infinite incompressible Newtonian non-magnetic fluid is considered. At the centre of the ferrofluid cylinder, a wire, with an electric current I passing through it, generates a steady axisymmetric azimuthal magnetic field (see figure 7). Gravity is ignored. Contrary to Canu and Renoult [4], the wire is hollow and a cold water flows inside. The conditions are no longer isothermal and temperature is supposed to be only r dependent. Only interfacial tension is assumed to be dependent on temperature. Finally, only thermal conduction is considered in the ferrofluid and the convection is neglected. Contrary to Arkhipenko *et al.* [7], no assumptions are made on the size of the ferrofluid layer and the cylindrical geometry is taken into account. Furthermore, a thermal balance of the experiment is performed.

This thermal balance is realised for a stable and not deformed ferrofluid cylinder. In the wire, at steady state, conduction is balanced by thermal production of energy:

$$\iint -\kappa_w \nabla T \cdot \boldsymbol{n} dS = \iiint P dV \tag{3}$$

with T, the temperature in K, κ_w, the thermal conductivity of wire in $W \cdot m^{-1} \cdot K^{-1}$, P, the energy production by Joule effect in $W \cdot m^{-3}$, $\boldsymbol{n}$, the normal to the wire surface, S, the wire surface, and V, the wire volume. Equation 3 leads to

$$\Delta T = -\frac{P}{\kappa_w} \tag{4}$$

Considering that T is only dependent on the radial coordinates r, the previous equation 4 gives the temperature profile in the wire

$$T = -\frac{P}{4\kappa_w} r^2 + A ln(r) + B \tag{5}$$

with A and B, constants. A is determined with the boundary condition at the inner wire radius $R_{w,i}$

$$-\kappa_w \frac{\partial T}{\partial r} \boldsymbol{e_r} \cdot \boldsymbol{n} S = \phi_{int} \quad \text{at} \quad r = R_{w,i} \tag{6}$$

with $S = 2\pi R_{w,i} L_w$, the inner wire surface and ϕ_{int}, the heat flux exchanged with the water flowing inside the wire. $\phi_{int} = \dot{Q} c_{p_{wat}} (T_{wat_o} - T_{wat_i})$ with $\dot{Q}$ the water mass flow rate in $kg \cdot s^{-1}$, $c_{p_{wat}}$ the water heat capacity in $J \cdot kg^{-1} \cdot K^{-1}$, T_{wat_i} the water temperature at the wire inlet and T_{wat_o} the water temperature at the wire outlet. At $r = R_{w,i}$, $\boldsymbol{n} = -\boldsymbol{e_r}$. Furthermore, the mass flow rate and the energy production are expressed as $\dot{Q} = \rho_{wat} (L_w / t_{io}) \pi R_{w,i}^2$ and $P = \rho_{e_w} I^2 / \left[\pi^2 \left(R_w^2 - R_{w,i}^2 \right)^2 \right]$, with ρ_{wat} the density of water, t_{io} the needed time for the water to cover the wire length, I the current, and ρ_{e_w}, the wire resistivity in $\Omega \cdot m$. With the temperature profile 5, we obtain

$$A = \frac{\rho_{e_w} I^2 R_{w,i}^2}{2\kappa_w \pi^2 \left(R_w^2 - R_{w,i}^2 \right)^2} + \frac{\rho_{wat} R_{w,i}^2 c_{p_{wat}}}{2\kappa_w} \frac{(T_{wat_o} - T_{wat_i})}{t_{io}} \tag{7}$$

Because a steady state is considered and because there is no energy production in the ferrofluid and surrounding fluid, the linear external heat flux ϕ_{ext} in $W \cdot m^{-1}$ is given by

$$\phi_{ext} = -\kappa_w \frac{\partial T}{\partial r} 2\pi R_w \quad \text{at} \quad r = R_w \tag{8}$$

where $\boldsymbol{n} = \boldsymbol{e_r}$ has been considered at $r = R_w$. Using relations 5 and 7,

$$\phi_{ext} = \frac{\rho_{e_w} I^2}{\pi \left(R_w^2 - R_{w,i}^2 \right)} - \pi \rho_{wat} R_{w,i}^2 c_{p_{wat}} \frac{(T_{wat_o} - T_{wat_i})}{t_{io}} \tag{9}$$

Then, the temperature profile in the ferrofluid is expressed as a function of ϕ_{ext}. In the same way than for the wire and considering no energy production inside the ferrofluid, the temperature profile is expressed as

$$T_1 = A_f ln(r) + B_f \tag{10}$$

with T_1 the temperature in the ferrofluid, and A_f and B_f two constants determined with the boundary conditions. Considering pure thermal conduction in the ferrofluid, pure thermal convection in the surrounding fluid and using thermal resistances in cylindrical coordinates, the temperature profile in the ferrofluid is given by

$$T_1 = T_{2,\infty} + \frac{\phi_{ext}}{2\pi}\left(\frac{1}{R_0 h_2} - \frac{ln\left(\frac{r}{R_0}\right)}{\kappa_1}\right) \tag{11}$$

with $T_{2,\infty}$ the ambient temperature, κ_1 the ferrofluid thermal conductivity in $W\cdot m^{-1}\cdot K^{-1}$ and h_2 the surrounding fluid convective coefficient in $W\cdot m^{-2}\cdot K^{-1}$.

To obtain the dispersion relation taking into account thermocapillary effects, the same methodology as for the isothermal case of Canu and Renoult [4] is employed. Only jump conditions of the momentum at the interface are modified

$$\begin{aligned}&\Pi_1 + \mu_0\int_0^H MdH + \frac{1}{2}\mu_0 M_{1n}^2 - (\boldsymbol{n}\cdot\tau_1)\cdot\boldsymbol{n}\\ &= P_2 - (\boldsymbol{n}\cdot\tau_2)\cdot\boldsymbol{n} + \sigma\boldsymbol{\nabla}\cdot\boldsymbol{n} \quad \text{at} \quad r = R_0+\zeta\end{aligned} \tag{12}$$

$$(\boldsymbol{n}\cdot\tau_2)\times\boldsymbol{n} - (\boldsymbol{n}\cdot\tau_1)\times\boldsymbol{n} = \nabla\sigma\times n \quad \text{at} \quad r = R_0+\zeta \tag{13}$$

with Π_1 the pressure in the ferrofluid modified by the magnetostrictive pressure, M the magnetisation, H the magnetic field, P_2 the pressure in the surrounding fluid, τ_i the viscous stress tensor in the fluid i, $\boldsymbol{n}$ the unit normal vector, σ the interfacial tension, and ζ the surface perturbation. Index 1 refers to ferrofluid and index 2 refers to the surrounding fluid. The grey terms are the modifications brought by the thermocapillary effect. Equation 12 is the same as in the isothermal case but σ is no longer constant and is expressed as $\sigma = \sigma_{2,\infty} - \sigma_c(T - T_{2,\infty})$ with $\sigma_{2,\infty}$ interfacial tension at $T = T_{2,\infty}$ and σ_c the interfacial tension gradient in $N\cdot m^{-1}\cdot K^{-1}$.
In the following, the relations are made dimensionless using $\sqrt{\rho_1 R_0^3/\sigma_{2,\infty}}$, R_0, $\sigma_{2,\infty}/R_0$, $\sigma_{2,\infty}$, $T_{2,\infty}$, $H_0 = I/2\pi R_0$ and the permeability of free space μ_0 as characteristic time, length, pressure, interfacial tension, temperature, magnetic field and magnetic permeability, respectively. Developing and linearising the equations, relations 12 and 13 become at first order

$$\begin{aligned}&\Pi_1 - \zeta N_{Bo,m} - 2Oh_1\frac{\partial u_{r1}}{\partial r} + 2Oh_1\eta_r\frac{\partial u_{r2}}{\partial r} - P_2 + \zeta + \frac{\partial^2\zeta}{\partial z^2}\\ &-\sigma_r\Theta_0\zeta - \sigma_r\Theta_0\frac{\partial^2\zeta}{\partial z^2} + \sigma_r\Theta + \sigma_r\zeta\frac{\partial\Theta_0}{\partial r} = 0 \quad \text{at} \quad r = 1\end{aligned} \tag{14}$$

$$\begin{aligned}&\eta_r\left(\frac{\partial u_{r2}}{\partial z} + \frac{\partial u_{z2}}{\partial r}\right) - \left(\frac{\partial u_{r1}}{\partial z} + \frac{\partial u_{z1}}{\partial r}\right)\\ &+\frac{\sigma_r}{Oh_1}\left(\frac{\partial\Theta}{\partial z} + \frac{\partial\Theta_0}{\partial r}\frac{\partial\zeta}{\partial z}\right) = 0 \quad \text{at} \quad r = 1\end{aligned} \tag{15}$$

with $\eta_r = \eta_2/\eta_1$ the viscosity ratio, $N_{Bo,m} = \left(\mu_0(\mu_r - 1)I^2\right)/\left(4\pi^2\sigma_{2,\infty}R_0\right)$ the magnetic Bond number, μ_r the relative magnetic permeability, $Oh_1 = \eta_1/\sqrt{\rho_1\sigma_{2,\infty}R_0}$ the Ohnesorge number, $\sigma_r = \sigma_c T_{2,\infty}/\sigma_{2,\infty}$, and $\Theta = (T - T_{2,\infty})/T_{2,\infty}$, a modified temperature. Index 0 refers to the basic state. Θ_0 corresponds to the modified temperature at basic state and is given by making dimensionless expression 11

$$\Theta_0 = \phi_{ext}\left(\frac{1}{Nu} - ln(r)\right) \tag{16}$$

with $Nu = h_2 R_0/\kappa_1$ the Nusselt number, and ϕ_{ext}, the dimensionless external heat flux given by

$$\phi_{ext} = \frac{\rho_{e_w} I^2}{2\kappa_1 T_{2,\infty}\pi^2\left(R_w^2 - R_{w,i}^2\right)} - \frac{\rho_{wat}R_{w,i}^2 c_{p_{wat}}}{2\kappa_1 T_{2,\infty}}\frac{(T_{wat_o} - T_{wat_i})}{t_{io}} \tag{17}$$

Then, to solve equations 14 and 15, the temperature inside the ferrofluid has to be known at first order. Neglecting the convective term, the temperature equation becomes

$$\frac{Pr}{Oh_1}\frac{\partial\Theta}{\partial t} - \Delta\Theta = 0 \tag{18}$$

with $Pr = \eta_1 c_{p_1}/\kappa_1$ the ferrofluid Prandtl number, and c_{p_1} the ferrofluid heat capacity. The solution of this equation 18 is

$$\Theta = \left[AI_0(nr) + BK_0(nr)\right]e^{ikz+\alpha t} \tag{19}$$

with n a modified wavenumber such as $n^2 = k^2 + \alpha(Pr/Oh_1)$. Two boundary conditions are needed to determine the constants A and B. They are

$$\Theta = 0 \quad \text{at} \quad r = \delta_w \tag{20}$$

$$-\boldsymbol{\nabla}\Theta\cdot\boldsymbol{n} = Nu\Theta \quad \text{at} \quad r = 1+\zeta \tag{21}$$

The first condition means that the temperature is not perturbed at the wire surface. The second relation comes from the equality at the interface between the conduction and the convection that occur in the ferrofluid and the surrounding fluid respectively. At first order, this second condition becomes

$$\frac{\partial\Theta}{\partial r} + Nu\Theta + \zeta\phi_{ext}(1 - Nu) = 0 \quad at \quad r = 1 \tag{22}$$

and the temperature has the following expression

$$\Theta = \frac{\phi_{ext}(Nu-1)\zeta_1}{\beta_1+\beta_2}\left[K_0(n\delta_w)I_0(nr) - I_0(n\delta_w)K_0(nr)\right]e^{ikz+\alpha t} \tag{23}$$

with ζ_1 such as $\zeta = \zeta_1 e^{ikz+\alpha t}$. β_1 and β_2 are defined in the list of notations below.
Finally, following the methodology of Canu and Renoult [4], the dispersion relation with thermocapillary effect is obtained:

$$\alpha^2+\alpha^2\rho_r\frac{\hat{b}_2K_0(k)}{I_0(k)-\hat{b}_1K_0(k)}+2Oh_1\alpha k\left[\frac{kI_0(k)-I_1(k)+\check{a}_1\left(l_1I_0(l_1)-I_1(l_1)\right)-\hat{b}_1\left(kK_0(k)+K_1(k)\right)-\check{b}_1\left(l_1K_0(l_1)+K_1(l_1)\right)}{I_0(k)-\hat{b}_1K_0(k)}\right.$$
$$\left.+\eta_r\frac{\hat{b}_2\left(kK_0(k)+K_1(k)\right)+\check{b}_2\left(l_2K_0(l_2)+K_1(l_2)\right)}{I_0(k)-\hat{b}_1K_0(k)}\right]-k\left(\left(1-\frac{\sigma_r\phi_{ext}}{Nu}\right)\left(1-k^2\right)\right.$$
$$\left.-\sigma_r\phi_{ext}\frac{\beta_1Nu+\beta_2}{(\beta_1+\beta_2)Nu}-N_{Bo,m}\right)\left[\frac{I_1(k)+\check{a}_1I_1(l_1)+\hat{b}_1K_1(k)+\check{b}_1K_1(l_1)}{I_0(k)-\hat{b}_1K_0(k)}\right]=0. \tag{24}$$

with the following notations

$$a=kI_0(k\delta_w)K_1(l_1\delta_w)+l_1I_1(k\delta_w)K_0(l_1\delta_w)$$
$$b=l_1I_0(l_1\delta_w)K_1(l_1\delta_w)+l_1I_1(l_1\delta_w)K_0(l_1\delta_w)$$
$$c=kK_0(k\delta_w)K_1(l_1\delta_w)-l_1K_1(k\delta_w)K_0(l_1\delta_w)$$
$$d=l_2I_1(k)K_1(l_1\delta_w)-l_2I_1(k\delta_w)K_1(l_1)$$
$$e=l_2K_1(k)K_1(l_1\delta_w)-l_2K_1(k\delta_w)K_1(l_1)$$
$$f=l_2I_1(l_1)K_1(l_1\delta_w)-l_2I_1(l_1\delta_w)K_1(l_1)$$
$$g=kI_0(k)K_1(l_1\delta_w)+l_1I_1(k\delta_w)K_0(l_1)$$
$$h=l_1K_1(k\delta_w)K_0(l_1)-kK_1(l_1\delta_w)K_0(k)$$
$$j=l_1I_0(l_1)K_1(l_1\delta_w)+l_1I_1(l_1\delta_w)K_0(l_1)$$
$$m=l_2K_0(l_2)K_1(k)-kK_1(l_2)K_0(k)$$
$$\beta_1=nI_1(n)K_0(n\delta_w)+nK_1(n)I_0(n\delta_w)$$
$$\beta_2=NuI_0(n)K_0(n\delta_w)-NuK_0(n)I_0(n\delta_w)$$
$$C_T=\frac{\sigma_r\phi_{ext}}{\alpha Oh_1}\frac{\beta_1Nu+\beta_2}{(\beta_1+\beta_2)Nu}$$
$$q=(2+C_T)k^2I_1(k)K_1(l_1\delta_w)-\left((1+C_T)k^2+l_1^2\right)I_1(k\delta_w)K_1(l_1)$$
$$w=(2+C_T)k^2K_1(k)K_1(l_1\delta_w)-\left((1+C_T)k^2+l_1^2\right)K_1(k\delta_w)K_1(l_1)$$
$$x=\left((1+C_T)k^2+l_1^2\right)I_1(l_1)K_1(l_1\delta_w)-\left((1+C_T)k^2+l_1^2\right)I_1(l_1\delta_w)K_1(l_1)$$
$$\gamma_1=\left(k^2-l_2^2\right)K_1(k)\left(K_1(l_2)(cg+ah)+K_0(l_2)(cd+ae)\right)l_2+\left(k^2+l_2^2\right)m(cd+ae)$$
$$\gamma_2=\left(k^2-l_2^2\right)K_1(k)\left(K_1(l_2)(cj+bh)+K_0(l_2)(cf+be)\right)l_2+\left(k^2+l_2^2\right)m(cf+be)$$
$$\check{a}_1=-\frac{(cq+aw)ml_2-\eta_r\gamma_1}{(cx+bw)ml_2-\eta_r\gamma_2}$$
$$\hat{b}_1=\frac{a+\check{a}_1b}{c}$$
$$\check{b}_1=-\frac{cI_1(k\delta_w)+aK_1(k\delta_w)+\check{a}_1\left(cI_1(l_1\delta_w)+bK_1(k\delta_w)\right)}{cK_1(l_1\delta_w)}$$
$$\hat{b}_2=\frac{K_1(l_2)(cg+ah)+K_0(l_2)(cd+ae)}{cmK_1(l_1\delta_w)}+\frac{\check{a}_1\left[K_1(l_2)(cj+bh)+K_0(l_2)(cf+be)\right]}{cmK_1(l_1\delta_w)}$$
$$\check{b}_2=\frac{(cd+ae)m}{cml_2K_1(l_2)K_1(l_1\delta_w)}+\check{a}_1\frac{(cf+be)m}{cml_2K_1(l_2)K_1(l_1\delta_w)}-\frac{\left[K_1(l_2)(cg+ah)+K_0(l_2)(cd+ae)\right]K_1(k)l_2}{cml_2K_1(l_2)K_1(l_1\delta_w)}-\check{a}_1\frac{\left[K_1(l_2)(cj+bh)+K_0(l_2)(cf+be)\right]K_1(k)l_2}{cml_2K_1(l_2)K_1(l_1\delta_w)}$$

Again, the terms modified by thermocapillary effect are coloured in grey. Four additional dimensionless parameters appear: the Nusselt number Nu, the Prandtl number Pr, the dimensionless interfacial tension gradient σ_r, and the dimensionless external heat flux ϕ_{ext}. Here, external heat flux means the heat flux directed from the wire towards the surrounding fluid. In figure 8, solutions of this dispersion relation are plotted for $Pr=56$, $Nu=1.7$, $\sigma_r=2.27$ and $\phi_{ext}=0.057$. Even if these values are realistic and based on what is encountered in the literature, no measurements of thermal parameters were performed in the experiment. These values were chosen to show that the discrepancy observed between theoretical predictions and experimental data can be explained by the thermocapillary effect. Furthermore, the flux value indicates that a heating from within (that means a heated wire) is necessary to stabilise the ferrofluid cylinder which is in contradiction with the comments of Arkhipenko *et al.*[7].

Another possible source of discrepancy could be the side effects, which are not modelled by the theory, at the cuvette walls to which the ferrofluid was attracted by capillarity. To verify these speculations, new experiments are necessary in which these parameters would be better controlled.

V. CONCLUSIONS

Experiments were performed to study the effect of modifying the wire radius on the stability of a ferrofluid cylinder in an azimuthal magnetic field. The ferrofluid is deposited on a hollow copper wire with an electric current running through it to create the azimuthal magnetic field. The ferrofluid is surrounded by a glycerol solution of approximately the same density to neglect the gravity effect. The ferrofluid cylinder is destabilised by passing from a high to a lower magnetic field intensity. Experimental data were analysed to extract the growth rate α and the wavelength λ of the deformation of the interface between the ferrofluid cylinder and the surrounding fluid. Several experiments were performed while varying the current I, the wire radius R_w and the ferrofluid cylinder radius

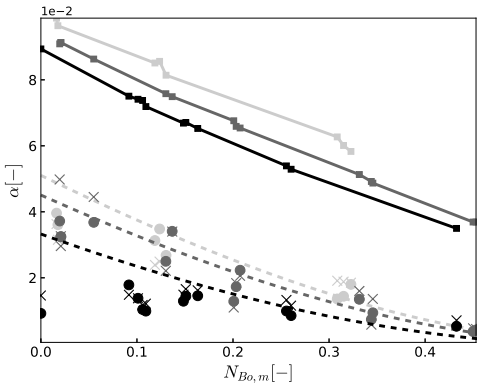

FIG. 8: Value of α as a function of $N_{Bo,m}$. The viscous theory of Canu and Renoult [4] is represented by solid lines with symbols. Crosses correspond to the experimental data obtained using the first method (peak maximum). Circles correspond to the experimental data obtained using the second method (interface length). Dashed lines correspond to the theory taking into account thermocapillary effect with $Pr = 56$, $Nu = 1.7$, $\sigma_r = 2.27$ and $\phi_{ext} = 0.057$. Light grey corresponds to the first series of measurements ($\delta_w = 0.444$ on average), intermediate grey to the second series ($\delta_w = 0.470$ on average) and black to the third series ($\delta_w = 0.524$ on average).

R_0 to study the influence of the dimensionless wire radius δ_w on the cylinder stability and respond to an issue raised in a previous paper[4]. The results confirm the theoretical predictions of Canu and Renoult [4] based on linear stability analysis under isothermal conditions, namely a decrease in the growth rate when δ_w increases. However, this theory does not predict our experimental data for the growth rate as effectively as with the experimental data of Arkhipenko *et al.* [2]. Even if uncertainties exist regarding the values of the fluid properties due to the thermal conditions of the experiment, they cannot entirely explain the discrepancy between the theoretical and experimental data. That is why an extended theory considering a thermocapillary effect has been developed. It was shown that this non-isothermal model can explain the discrepancy observed, by assuming realistic heat transfers in the present experiment. All models and our experiments agree with the fact that when δ_w increases, the growth rate decreases. These new experiments on this subject allowed us to resolve an issue raised by our previous study on the effect of the wire on the ferrofluid column stability.

Other experiments are still necessary with a better control on the fluid properties, wire cooling and other side effects, which can be sources of the observed discrepancy between the isothermal theory and the experiments. Several ferrofluids and surrounding fluids could also be used to study the effect of the fluids viscosity.

ACKNOWLEDGMENTS

This work was supported by LabEx EMC3 through the INFEMA (INstabilities of FErrofluid flows in MAgnetic fields) project, jointly conducted by LOMC (Normandie Univ, UNIHAVRE, CNRS) and CORIA laboratories. The authors would like to thank the Mechanical Engineering and Manufacturing Department and the Metrology and Instrumentation Division of the CORIA laboratory for their support regarding the experimental setup.
The authors report no conflict of interest.

[1] R. E. Rosensweig, *Ferrohydrodynamics*, Cambridge monographs on mechanics and applied mathematics (Cambridge University Press, Cambridge ; New York, 1985).
[2] V. I. Arkhipenko, Y. D. Barkov, V. G. Bashtovoi, and M. S. Krakov, "Investigation into the stability of a stationary cylindrical column of magnetizable liquid," Fluid Dyn **15**, 477–481 (1981).
[3] R. Canu and M.-C. Renoult, "Linear stability analysis of a newtonian ferrofluid cylinder under a magnetic field," J. Fluid Mech. **915**, A137 (2021).
[4] R. Canu and M.-C. Renoult, "Linear stability analysis of a newtonian ferrofluid cylinder surrounded by a newtonian fluid," Journal of Fluid Mechanics **927** (2021), 10.1017/jfm.2021.782, publisher: Cambridge University Press.
[5] S. Ferguson Briggs and A. Mestel, "Linear stability of a ferrofluid centred around a current-carrying wire," Journal of Fluid Mechanics **942**, A20 (2022).
[6] E. Bourdin, J.-C. Bacri, and E. Falcon, "Observation of Axisymmetric Solitary Waves on the Surface of a Ferrofluid," Physical Review Letters **104**, 094502 (2010).
[7] V. I. Arkhipenko, Y. D. Barkov, V. G. Bashtovoi, M. S. Krakov, and M. I. Pavlinov, "Effects of viscosity and nonuniform heating on the break-up of a cylindrical layer of magnetized liquid," Magnetohydrodynamics **17**, 232–237 (1981).
[8] X.-W. Gong, D.-M. Mo, C.-M. Wu, and Y.-R. Li, "Linear-stability analysis of thermocapillary-buoyancy convection in annular two-layer system with a radial temperature gradient," International Communications in Heat and Mass Transfer **66**, 58–62 (2015).
[9] H. Liu, Z. Zeng, L. Yin, Z. Qiu, and L. Qiao, "Influence of aspect ratio on the onset of thermocapillary flow instability in annular pool heated from inner wall," International Journal of Heat and Mass Transfer **129**, 746–752 (2019).
[10] H. Liu, Z. Zeng, Z. Qiu, L. Yin, and Y. Xiao, "Effect of rotating magnetic field on instabilities of thermocapillary flow in a Czochralski silicon melt pool," Physics of Fluids **32**, 104106 (2020).
[11] H.-M. Li, L. Feng, W.-Y. Shi, and M. K. Ermakov, "Instabilities of thermocapillary-buoyant-Coriolis flow of medium Prandtl fluid in a slowly rotating annular pool," International Communications in Heat and Mass Transfer **130**, 105801 (2022).
[12] Y. Wang, L. Zhang, H. Liu, L. Yin, Y. Xiao, Y. Liu, and Z. Zeng, "Effect of Prandtl number on the flow instabilities in thermocapillary liquid bridges between two coaxial disks with different radii," International Journal of Heat and Mass Transfer **205**, 123895 (2023).
[13] M. K. Smith and S. H. Davis, "Instabilities of dynamic thermocapillary liquid layers. Part 1. Convective instabilities," Journal of Fluid Mechanics **132**, 119–144 (1983), publisher: Cambridge University Press.
[14] I. Hashim, H. Othman, and S. A. Kechil, "Stabilization of thermocapillary instability in a fluid layer with internal heat source," International Communications in Heat and Mass Transfer **36**, 161–165 (2009).
[15] Z. Ding and Q. Liu, "Linear instability analysis of thermocapillary convection in a bilayer system," International Journal of Heat and Mass Transfer **62**, 63–72 (2013).
[16] K.-X. Hu, M. He, Q.-S. Chen, and R. Liu, "Effect of gravity on the stability of viscoelastic thermocapillary liquid layers," International Journal of Heat and Mass Transfer **123**, 776–786 (2018).
[17] S. Chattopadhyay, A. Mukhopadhyay, A. K. Barua, and A. K. Gaonkar, "Thermocapillary instability on a film falling down a non-uniformly heated

Accepted to Phys. Fluids 10.1063/5.0169793

slippery incline," International Journal of Non-Linear Mechanics **133**, 103718 (2021).
[18]S. Mukhopadhyay and A. Mukhopadhyay, "Surface wave and thermocapillary instabilities on flowing film under the sway of Hall viscosity," Physica D: Nonlinear Phenomena **439**, 133404 (2022).
[19]J.-J. Xu and S. H. Davis, "Instability of capillary jets with thermocapillarity," Journal of Fluid Mechanics **161**, 1–25 (1985), publisher: Cambridge University Press.
[20]W. R. Hu and N. Imaishi, "Thermocapillary flow in an annular liquid layer painted on a moving fiber," Int. J. Heat Mass Transfer (2000).
[21]I. I. Ryzhkov and V. M. Shevtsova, "Thermocapillary instabilities in liquid columns under co- and counter-current gas flows," International Journal of Heat and Mass Transfer **55**, 1236–1245 (2012).
[22]M.-C. Renoult, P. Carles, S. Ferjani, and C. Rosenblatt, "2D Rayleigh-Taylor instability: Interfacial arc-length vs. deformation amplitude," EPL (Europhysics Letters) **101**, 54001 (2013).